Доклади на Българската академия на науките
Comptes rendus de l'Académie bulgare des Sciences

Tome 66, No 1, 2013

SCIENCES ET INGENIERIE

Mécanique

IDENTIFICATION OF MECHANICAL CHARACTERISTICS OF AN AMORPHOUS METALLIC MATERIAL

Nikola Nikolov, Dessislava Pashkouleva, Ana Yanakieva

(*Submitted by Corresponding Member A. Baltov on June 25, 2012*)

Abstract

The research aims to identify the mechanical characteristics of an amorphous metallic alloy as cast and after heating, and suggests the effects of applications of such a material as a filler in composites. The amorphous state of Zirconium-based alloy is obtained through melt-spinning and is identified by X-ray diffraction (XRD). The region of heating is identified by Differential Scanning Calorimetry (DSC). Two types of samples are tested under one-axial tension. The first are made of the alloy in amorphous state. The others are made of the same alloy but after heating and cooling at air, which may provoke changes in the amorphous structure to formation of nanocrystals. For the two types of samples, the stress-strain diagrams and parameters of bilinear material models are drawn applying FEM-simulation of the observed tensile behaviour. The obtained stress-strain diagrams are illustratively compared with a similar one for conventional copper.

The results could be useful in the design of composite materials with properties given in advance for each material phase. That is demonstrated by an analytical example predicting the effective modulus of elasticity for two-phased composite material.

Key words: amorphous materials, nanocrystalline materials, tensile experiments, FE-modelling, two-phased composites

1. Introduction. During the last 30–40 years, with the development of new production technologies and corresponding research techniques, the influence of atomic radius on the formation of nonconventional metallic structures, including

The study was supported by project ДУНК-01/3/2009.

amorphous and nanocrystalline, has become a subject of advanced investigations. In these materials, the lack of conventional crystal-lattice structures ordered in long distances appears as crucial for their mechanical behaviour and determines the operation of specific mechanisms of plastic deformation.

A detailed review of the fundamental mechanisms of deformation and fracture acting in amorphous and nanocrystalline metallic materials could be found in [1]. The local directional bonding among the different atoms and formation of groups of atoms are critical to the obtaining of amorphous solid state, formation of nanocrystals, as well as to their stabilization and plastic behaviour. The plastic deformation in such kind of structures is influenced by both stresses – shear and normal. In many cases, the deformation appears as an inhomogeneous through plastic strains concentrated in localized volumes and shear bands [2].

In between the ensembles of mechanisms determining the macroscopic yield and failure behaviour of metallic amorphous materials operate: 1) nucleation of shear transformation zones, where the atoms are rearranged in order to compensate the shear strains; 2) propagation of these zones and their transformations in shear bands and subsequent growth; 3) adiabatic heating in locally-deformed regions; 4) nucleation of nanocrystals, inside or around shear bands; 5) nucleation of nano-sized voids in shear bands; 6) coalescence of voids causing failure. The theories describing the deformation behaviour of amorphous and nanocrystalline materials include viscose-elastic response at low applied stresses, sharp dynamical transition to viscose-plastic response with increasing stress above the yield stress limit, followed by strain hardening and plastic deterioration based on the so-called shear-transformation zones [3].

2. Theoretical basis of the material's chemical content. In a metallic alloy composition, the difference in the atomic radii of chemical elements, electronic structures of atoms, as well as the atomic concentrations in the alloy mass and alloy volume play essential roles during the operating of mechanisms pointed out in the previous section. For this reason, recently to the well-known three basic rules for synthesis of amorphous-nanocrystalline alloys (which include multi-component systems with more than three elements; difference in atomic radii above 12% and negative heat of mixing of three basic elements [4]), new two criteria characterizing the atomic structures and geometry of the alloys have been added. They include criterion of average valance electron per atom e/a ratio $\sim$ 1.4 and constant atomic size ($\mathrm{Ra} \sim 1.4$ nm) of the alloy [5].

Generally, the multicomponent amorphous Zr-based alloys can change their structures through thermal treatment in the supercooled liquid region, which is defined by difference between both – the temperature crystallization Tx and the temperature glasstransition Tg. The alloys form different nanocrystals and icosahedral quasi-crystalline precipitates in the amorphous matrix depending on the different chemical compositions. For example, thermal treatment of $Zr_{69.5}Al_{7.5}Cu_{12}Ni_{11}$ above Tg leads to forming of quasi-crystalline phases with

fine sizes in the range of 50–100 nm [5]. The dispersion of such particles in the amorphous matrix improves the mechanical characteristics.

Taking into consideration the above-mentioned theoretical statements, both the temperatures Tg and Tx of the alloy $Zr_{65}Al_{10}Cu_{15}Ni_{10}$ are mathematically modelled depending on additions from 1 to 10 atomic % of element with atomic radius in the range of 0.138–0.174 nm [4]. Gallium (Ga) possesses atomic radius of 0.1673 nm, which is close to these of Nickel (Ni) and Titanium (Ti), respectively 0.162 and 0.165 nm. Aluminium (Al) and zirconium (Zr) possess atomic radii of 0.1582 and 0.1771, i.e. the Ga-atomic radius appears as an average in between them. On the other hand, Ga and Al belong to one and the same group in the periodic table and they have equal valence of +3. The Ga-addition changes the e/a-ratio of the system, which is $e/a = 1.39$ [5]. Through Ga-addition to $Zr_{65}Al_{10}Cu_{15}Ni_{10}$, the mentioned circumstances give opportunities to predict the obtaining of new amorphous alloy with large ability to nanocrystalization.

This elaboration aims to identify the structure, thermal properties and mechanical characteristics of the alloy $Zr_{58}Al_{10}Cu_{15}Ni_{10}Ga_7$, which is predicted [4] as amorphous with glass-forming ability in supercooled liquid region defined from Tg = 680 K and Tx = 760 K, as well as to outline possible applications based on its specific characteristics.

3. Experiments and finite element modelling. Following [4], in laboratory conditions, 7 At% of Ga are added to the alloy $Zr_{65}Al_{10}Cu_{15}Ni_{10}$ replacing Zr and a new alloy $Zr_{58}Al_{10}Cu_{15}Ni_{10}Ga_7$ is synthesized. Experimental specimens are obtained in the form of ribbons with thicknesses of 32 μm and width of 1.25 mm through melt-spinning.

The alloy structure is identified as amorphous by X-ray diffraction and the obtained X-ray pattern is presented in Fig. 1*a*. As it can be seen, the XRD-pattern of $Zr_{58}Al_{10}Cu_{15}Ni_{10}Ga_7$ ribbons consists of only broad diffraction maxima without any sharp Bragg's peak, indicating that the sample is an amorphous within XRD detection limit.

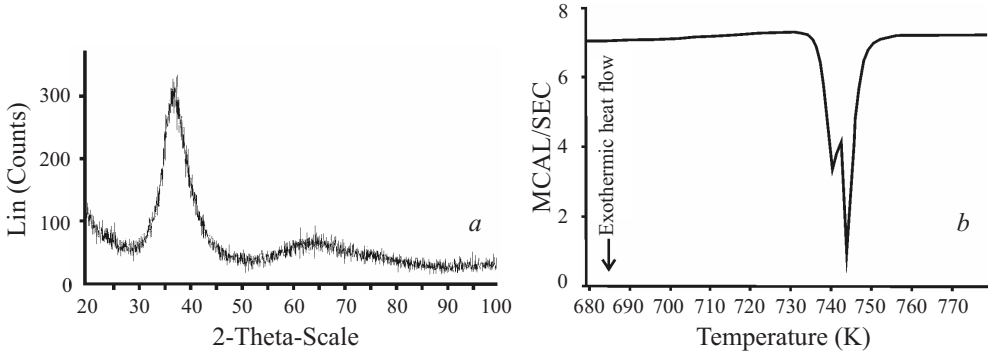

Fig. 1. *a*) X-ray diffraction pattern; *b*) thermogram of the alloy $Zr_{58}Al_{10}Cu_{15}Ni_{10}Ga_7$

Differential Scanning Calorimetry (DSC) is performed in order to investigate the structural transformations and establish glass transition and crystallization temperatures. The melting (solidus) points, melting temperature ranges and melting enthalpy are determined in argon atmosphere by differential scanning calorimeter Perkin Elmer DSC 2C applying constant heating rate of 20 K/min, in the range from 320 to 1000 K. The tolerance of assigned temperature and its reading is ±0.5 K.

The calorimetric results obtained for the alloy $Zr_{58}Al_{10}Cu_{15}Ni_{10}Ga_7$ are shown in Fig. 1*b*. The crystallization range read on the thermogram is from 732 to 756 K with maximum at 744 K. The crystallization enthalpy is $\Delta H = -12.24$ cal/gr. The glass transition and crystallization temperatures calculated by mathematical models [4] are Tg = 680 K and Tx = 760 K. Their difference determines the permissible region of heat treatment aiming change in the amorphous structure, Fig. 1*a*, respectively above 680 and below 760 K, Fig. 1*b*. The calculated derivation in the mathematically modelled and experimentally measured values of Tx is in the order of 2%.

One-axial tensile tests are carried out to study the mechanical properties of the investigated material. A computer-controlled testing device type "Instron" is used. The maximum load range is up to 500 N. The speed of testing is 0.13 mm/s. The total length of the test piece is 60 mm and the work length is 18 mm. Such a short length ensures comparative homogeneity of the structure loaded at tension. Three experiments are carried out with two types of samples. The first of them are prepared from such a material as it is obtained in amorphous state after rapid quenching through the melt-spinning, Fig. 1*a*. The other three samples are prepared from the same amorphous material but after heating over 680 K (Fig. 1*b*) for 30 s in the supercooled liquid region. Such a thermal treatment should lead to nucleation of nanocrystals and as a consequence increasing plastic strains. For the couple of experiments, the results read for "Force-displacement" are averaged

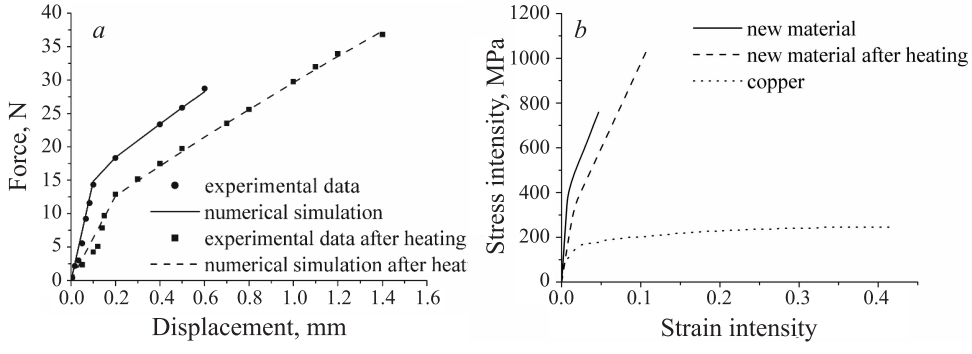

Fig. 2. *a*) Experimental and numerical results for force-displacement at one-axial tension; *b*) Stress-strain intensity in the middle part of ribbon-samples under tension

and shown by symbols in Fig. 2*a*. They deviate in maximal ranges of 5–10%. A numerical simulation of the material's behaviour at tension is accomplished taking into account the experimentally-obtained dependencies "Force-displacement" given with symbols in Fig. 2*a*. 3-D finite elements Visco107 are used to model the samples. 18 030 nodes are defined in the volume of a sample. Bilinear material's model is applied for the two kinds of samples. The following model parameters including: module of elasticity E, Poisson ratio ν, yield stress limit σ_P, tangentional module E_T and fracture stress limit σ_{fract} are identified simulating the experimentally observed material's tension behaviour, Table 1. During the simulation, the tension load is applied in 12 steps for non-thermo-treated amorphous samples and in 18 steps for the thermo-treated ones. In Figure 2*b*, the stress-strain diagrams of the two materials are given. They are obtained from stress-strain states of 1817 nodes located in the middle part of samples in limits of 6 mm, where the tenso-sensors should be attached at the experiment. The values given in Table 1 are identified as parameters' values of the assumed materials models for the two kinds of samples. In the last two columns, the obtained fracture stresses and strains, seen also in Fig. 2*b*, are given.

T a b l e 1

Parameters of physical models of amorphous and nanocrystalline ribbons

Sample	E, GPa	ν	σ_P, MPa	E_{T}, MPa	σ_{fract}, MPa	$\varepsilon_{\text{fract}}$
Before heating	70	0.36	420	1.25×10^4	1038	0.108
After heating	30	0.36	333	1.15×10^4	758	0.047

In Table 1 and Fig. 2*b*, an increase in 56% of plastic strains $\varepsilon_{\text{fract}}$ of amorphous samples is read as consequence of changes in the material's structure after the heating for 30 s. In order to compare illustratively the observed and modelled mechanical behaviour of the amorphous alloy, in the same figure the stress-strain diagram of a sample made of conventional copper wire with cross section equal to that of the tested samples is shown.

In Figure 2*b*, the observed plastic effect above strains 0.007 and 0.016 up to 0.05 and 0.1 respectively for the two type samples is not often seen in the mechanical behaviour of amorphous metallic structures. The revealed plasticity could be explained by some processes of nucleation of nanocrystals, commented in Sections 1 and 2. They could be developed because of local adiabatic heating caused by the mechanical loading. Similar effects are reported in [6] and are observed under tension of samples made of Zr-Al-Cu-based amorphous alloy. As a reason for appearance of plastic effects, the nucleation of a great number of nanocrystals embedded in the glassy matrix and their growths to diameters of up to 10–50 nm is commented.

4. Analytical example of a two-phased composite material. Both materials obtained by the presented technology and possessing structure (Fig. 1*a*) thermal (Fig. 1*b*) and mechanical properties (Fig. 2) as the above-identified could be useful with different forms as a second phase in preparing composite materials. In general, there are three kinds of fillers in nanocomposites: (1) cylinder-like nanofibres (aligned or randomly oriented); (2) disc-like plates; (3) spheroid-like particles. For each of them, a number of micromechanical models can be found in literature predicting the modulus of elasticity. The widely-used ones applicable to this research are:

– *Voigt upper bound and Reuss lower bound* (*V–R model*) – for aligned fibres applying uniaxial loading in fibre direction and transverse loading [7];

– *Hashin and Shtrikman upper and lower bounds* (*H–S model*) – for composites with macroscopical isotropy and quasi-homogeneity and without limitation of the shape of the filler [8];

– *Halpin–Tsai model* (*H–T model*) – for aligned fibre-reinforced composites [9, 10].

– *Hui–Shia model* (*H–S model*) is used to predict the overall module of composites with aligned fillers, especially considering fibre-like and disc-like fillers [11];

– *Wang–Pyrz model* (*W–P model*) – for composites with isotropic matrices and randomly-oriented transversely-isotropic spheroids. The model provides expressions for the overall bulk and shear module using the Mori–Tanaka method [12].

Example. In the presented work, the *H–T model* has been chosen to estimate the effects of amorphous metallic fillers in a cement matrix. The longitudinal E^l and transverse E^t module of *H–T model* are as follows [9, 10]:

$$E^l = \frac{1 + 2\,\xi\, V_f \eta^l}{1 - V_f \eta^l}\, E_m \quad \text{and} \quad E^t = \frac{1 + 2 V_f \eta^t}{1 - V_f \eta^t}\, E_m, \tag{1}$$

where $\xi = \dfrac{l}{d}$ for cylinder-like nanofibres (l and d are the length and diameter of the fibre) or $\xi = \dfrac{D}{t}$ for the disc-like plate fillers (D and t are plate diameter and thickness) and η^l and η^t read

$$\eta^l = \frac{E_f - E_m}{E_f + 2\,\xi\, E_m} \quad \text{and} \quad \eta^t = \frac{E_f - E_m}{E_f + 2E_m}. \tag{2}$$

The assumed filler shape is disc-like with the following geometric and material values: 1) the aspect ratio of the nanoparticles is $\xi = 2, 3, \ldots, 6$; 2) the matrix is cementitious, with material modulus $E_m = 11.2$ GPa according to [13] and the filler modulus is $E_f = 30$ GPa according to the results found in the current research and given in Table 1; 3) the volume of fraction attains different values $V_f = 0.1, 0.2, \ldots, 0.5$, Fig. 2*a*.

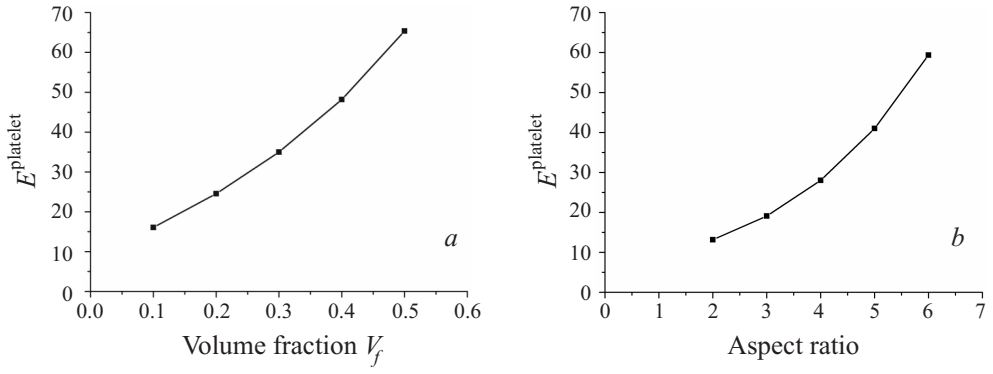

Fig. 3. Effective modulus vs volume fraction *a*) and aspect ratio *b*)

After finding the longitudinal and transverse modules of elasticity, the effective modulus of the composite in three orthogonal directions is found using the relation

$$E^{\text{platelet}} = 0.49E^l + 0.51E^t. \tag{3}$$

The results in Fig. 3 indicate an increase of the effective modulus with increase of both volume of fraction and aspect ratio by an average value of 50% for each step.

5. Conclusions. The identified material's mechanical behaviour (Fig. 2*b*) is dependent on the amorphous structure, Fig. 1*a*. Such a structure could be manipulated by heating in a supercooled liquid region established in Fig. 1*b*, which will be the topic of future research. Both resulting mechanical behaviours are different from those of conventional materials. Used in composites, the new materials increase the effective elastic modulus several times, Fig. 3.

REFERENCES

[1] Schuh C., T. Hufnagel, U. Ramamurty. Acta Mater., **55**, 2007, No 12, 4067–4109.

[2] Li J., G. Shan, K. Gao, L. Qiao, W. Chu. Mater. Science & Eng., **A354**, 20037, Nos 1–2, 337–343.

[3] Lund A., C. Schuh. Intermetallics, **12**, 2004, Nos 10–11, 1159–1165.

[4] Nikolov N. Technical Ideas, **XLI**, 2004, No 4, 67–79.

[5] Chen W., Y. Wang, J. Qiang, C. Dong. Acta Mater., **51**, 2003, No 7, 1899–1907.

[6] Pauly S., G. Liu, S. Gorantla, G. Wang, U. Kuhn, D. H. Kim, J. Eckert. Acta Mater., **58**, 2010, No 14, 4883–4890.

[7] Voigt W. Ann. Phys., **38**, 1889, No 3, 573–587.

[8] Hashin Z. J. Appl. Mech., **50**, 1983, No 5, 481–505.

[9] Halpin J. C. Premier on composite materials: analysis, Technomic Publishing Company, 1984.
[10] Hill R. J. Mech. Phys. Solids, **12**, 1964, No 4, 199–212.
[11] Qiu Y. P., G. L. Weng. Int. J. Eng. Sci., **28**, 1990, No 11, 1121–1137.
[12] Wang J., R. Pyrz. Compos. Sci. Tech., **64**, 2004, Nos 7–8, 925–934.
[13] MatWeb – Source for Materials Information, http://www.matweb.com/

Institute of Mechanics
Bulgarian Academy of Sciences
Acad. G. Bonchev Str., Bl. 4
1113 Sofia, Bulgaria
e-mail: n.nikolov@imbm.bas.bg